Spherically-Clustered Porous Au–Ag Alloy Nanoparticle Prepared by Partial Inhibition of Galvanic Replacement and Its Application for Efficient Multimodal Therapy

Hongje Jang and Dal-Hee Min*

Department of Chemistry, Center for RNA Research, Institute for Basic Sciences (IBS), Seoul National University, Seoul, 151-747, Republic of Korea

ABSTRACT The polyvinylpyrrolidone (PVP)-coated spherically clustered porous gold–silver alloy nanoparticle (PVP-SPAN) was prepared by low temperature mediated, partially inhibited galvanic replacement reaction followed by silver etching process. The prepared porous nanostructures exhibited excellent photothermal conversion efficiency under irradiation of near-infrared light (NIR) and allowed a high payload of both doxorubicin (Dox) and thiolated dye-labeled oligonucleotide, DNAzyme (FDz). Especially, PVP-SPAN provided 10 times higher loading capacity for oligonucleotide than conventional hollow nanoshells due to increased pore diameter and surface-to-volume ratio. We demonstrated highly efficient chemo-thermo-gene multitherapy based on codelivery of Dox and FDz with NIR-mediated photothermal therapeutic effect using a model system of hepatitis C virus infected human liver cells (Huh7 human hepatocarcinoma cell line containing hepatitis C virus NS3 gene replicon) compared to conventional hollow nanoshells.

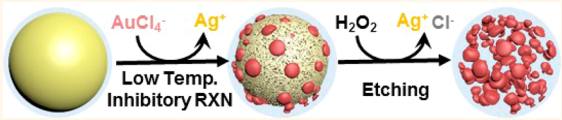

KEYWORDS: drug delivery · galvanic replacement · hepatitis C · photothermal therapy · nanomaterials

The galvanic replacement reaction is one of the most widely employed approaches to prepare hollow nanoshell structures by converting sacrificial metal nanocrystals into more noble metals such as Au, Pt, and Pd.[1−4] Among them, replaced Au nanoshells have found their high potential for diverse biomedical applications due to higher surface area compared to filled nanomaterials, low cytotoxicity, well-established bioconjugation strategies, and unique optical properties.[5−8] In principle, based on the difference in electrode potential of sacrificial and replacing metal elements, replacing metal ions get simultaneously reduced and deposited in the form of metal, while template metal nanoparticles dissolve out. During the replacing process, fast reaction time of galvanic replacement combined with the different relative diffusion rates of two metal elements enables the formation of hollow nanoshells.[9,10] However, AgCl, a byproduct generated during the galvanic replacement, deposits onto Ag surface and subsequently disturbs the formation of clean nanoshell morphology. In order to avoid this interference, the reaction is generally carried out at about 80 °C.[9] Conventional hollow Au nanoshells or nanocages are widely used in the application fields of catalyst, drug delivery, and stimulation triggered drug release by using their physicochemical properties and attractive structure of interior vacancy and high surface area than general nanospheres.[11−15]

Recently, interesting approaches of galvanic replacement reaction were reported such as antigalvanic replacement reaction between Ag and Au,[16,17] unconventional galvanic replacement of surface-limited templates,[18] and tailoring replacement with controlled number of voids.[19] Especially, a strategy of tailored galvanic replacement reaction in which the addition of HCl causes rapid precipitation of AgCl onto nanoparticle surface, generating removable secondary templates, allowed the formation of a greater variety of nanostructures such as hollow nanocages, dimers, multimers, and popcorn-shaped nanostructures.

* Address correspondence to dalheemin@snu.ac.kr.

Received for review November 14, 2014 and accepted January 5, 2015.

Published online January 05, 2015
10.1021/nn506492s

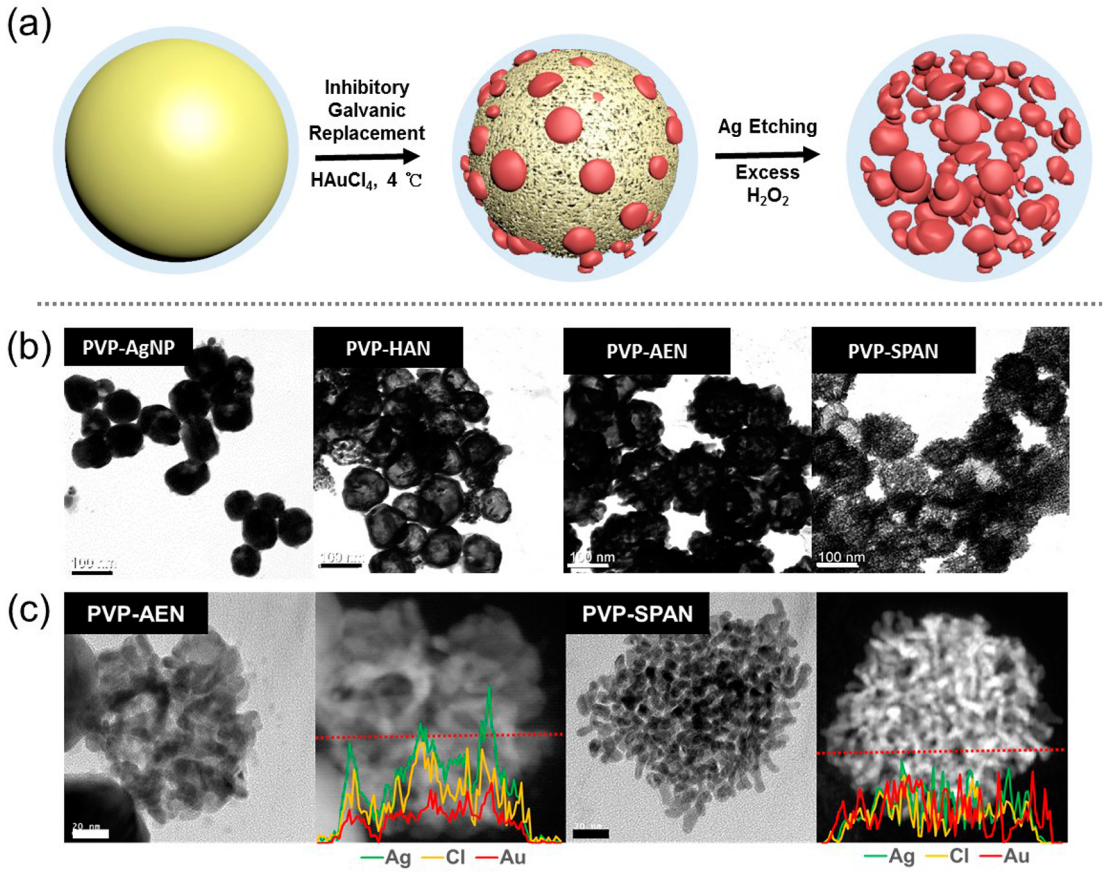

Figure 1. Schematic illustration and TEM images of PVP-SPAN prepared by inhibitory galvanic replacement reaction followed by hydrogen peroxide etching. (a) Scheme illustrated that low-temperature-induced rapid AgCl deposition generated the embedded gold nanoparticles in template Ag element and following etching process enabled the formation of spherically clustered nanostructure. (b) TEM images of PVP-AgNP, PVP-HAN, PVP-AEN, and PVP-SPAN exhibited morphological changes that occurred during the preparation. Scale bar is 100 nm. (c) HR-TEM and HAADF-STEM/EDS analysis of PVP-AEN and PVP-SPAN clearly showed the etching mediated transformation into spherically clustered porous structure and decrease in relative contents of Ag and Cl after etching process. Scale bar is 20 nm.

Here, we report galvanic replacement reaction of polyvinylpyrrolidone (PVP)-coated Ag nanoparticles, partially inhibited by low temperature, followed by sequential etching using hydrogen peroxide to form PVP-coated porous gold−silver alloy nanoparticle (PVP-SPAN) presenting spherically clustered nanoparticle structures (Figure 1a). Surface PVP coating of template Ag nanoparticle acts as a barrier preventing outgrowth of replaced nanostructure and a structural supporting material inhibiting collapse of the nanostructure. The formation of the clustered porous nanostructure is achieved by two step processes. First, the galvanic replacement reaction carried out at low temperature induces rapid AgCl deposition onto Ag surface around reaction sites to compete with continued replacement, resulting in local prevention of further galvanic replacement reaction. Second, after the replacement reaction is complete, the etching of remaining Ag and AgCl by excess hydrogen peroxide etchant reveals the embedded spherically clustered nanostructures (Figure S1a). To investigate potential applications of the prepared PVP-SPAN as a drug delivery vehicle, we conjugated doxorubicin (Dox, an anticancer drug which inhibits topoisomerase II activity by intercalating into DNA) *via* Schiff base imine linkage formation onto chemically introduced aldehyde groups in PVP coating and thiolated FAM-labeled 10−23 DNAzyme (FDz, catalytic DNA molecule designed to sequence-specifically cleave target RNA and thus silence the expression of NS3 gene of hepatitis C virus)[20,21] by chemisorption onto gold surface of the nanocarriers. We found that the PVP-SPAN enabled 10 times higher FDz payload compared to PVP-coated hollow Au−Ag nanoshell without large pores (PVP-HAN) while providing similar loading capacity for Dox. In addition, efficient photothermal conversion of PVP-SPAN based on preferential absorption of near-infrared (NIR) light showed high efficacy for photothermal therapy. To the best of our knowledge, this report is first to demonstrate a new synthetic strategy of PVP-SPAN by low-temperature-induced preventive galvanic replacement reaction and its high potential for chemo-thermo-gene multimodal therapy based on high porosity and favorable photothermal property effective at NIR region.

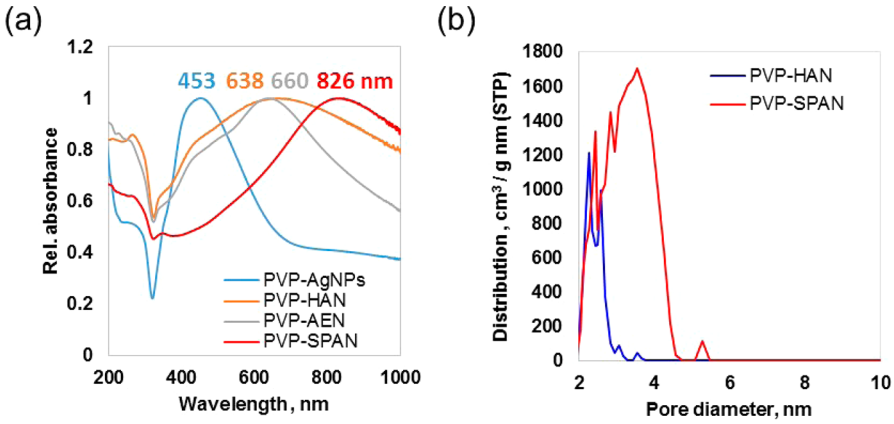

(c)

	Mean pore size (nm)	BET surface area (m^2/g)	Pore volume (mL/g)
PVP-HAN	2.3	64	0.13
PVP-SPAN	3.7	189	0.49

Figure 2. Characterization of PVP-AgNP, PVP-HAN, PVP-AEN, and PVP-SPAN. (a) UV−vis spectra showed the distinctive structure formation through conventional and inhibitory galvanic replacement of template PVP-AgNP. (b and c) Nitrogen adsorption data revealed that pore diameter of PVP-SPAN (3.7 nm) was larger than PVP-HAN (2.3 nm). Scale bar is 100 nm. Abbreviations are: PVP-AgNP: PVP-coated silver nanoparticle; PVP-HAN: PVP-coated hollow Au−Ag alloy nanoshell without large pore; PVP-AEN: PVP-coated Au embedded nanoparticle; and PVP-SPAN: PVP-coated spherically clustered porous Au−Ag alloy nanoparticle (PVP: polyvinylpyrrolidone).

RESULTS AND DISCUSSION

We first prepared sacrificial PVP-AgNP by previously reported polyol synthesis with slight modification.[22] Galvanic replacement reaction was then carried out by addition of 50 μL of 1 mM $AuCl_4^-$ solution in distilled water to as-synthesized PVP-AgNP (1 mL, 100 pM) at 4 °C, which is the lowest temperature needed to induce local deposition of AgCl. After 30 min, the mixture was purified by centrifugation and washed with distilled water to remove dissolved Ag ions and salts. The etching reaction by hydrogen peroxide was next performed to reveal the morphology of the replaced Au nanostructures. Transmission electron microscopy (TEM) images showed spherical nanoparticles with rough surface morphology and spherically clustered nanoparticles before and after the etching process, respectively (Figure 1b). High-resolution TEM (HR-TEM) and high-angle annular dark-field scanning transmission electron microscopy/energy-dispersive spectrometry (HAADF-STEM/EDS) supported the embedded structure formation (PVP-AEN, Au embedded nanoparticle) and etching mediated revealing of spherically clustered Au−Ag alloy nanoparticles (PVP-SPAN) (Figure 1c). According to dynamic light scattering (DLS) measurement and TEM images, hydrodynamic diameter was slightly larger than the size estimated from TEM images (n = 50) (PVP-AgNP: 169.4 and 135.1 nm, PVP-AEN: 176.6 and 153.2 nm, PVP-SPAN: 237.7 and 177.8 nm, respectively obtained from DLS and TEM) (Figure S2).

To investigate the effect of temperature in the formation of PVP-SPAN, we ran the same galvanic replacement reactions at varying temperatures, 4, 20, 40, and 80 °C. TEM images showed that the replacement reaction carried out at low temperature (≤20 °C) induced the formation of rough clustered nanoparticle morphology. However, smooth hollow nanoshells were mostly observed at higher temperature (≥40 °C). Through the etching process, these nanostructures converted into spherically clustered porous nanoparticles and hollow nanoshell/net structures, respectively (Figure S1b). The result suggests that temperature is a key parameter in the present strategy for the preparation of spherically clustered gold embedded nanostructures.

UV−vis spectra of PVP-AgNP, PVP-HAN, PVP-AEN, and PVP-SPAN exhibited surface plasmon resonance maxima at 453, 638, 660, and 826 nm, respectively (Figure 2a). This red-shift is due to the formation of hollow structure and rough morphological surface by galvanic replacement and transformation into connected porous cluster structure by etching. Nitrogen adsorption measurement clearly showed larger pore diameter of PVP-SPAN (3.7 nm) compared to PVP-HAN (2.3 nm). The measured surface area and pore volume of PVP-SPAN (189 m^2/g and 0.49 mL/g) were about 3-fold higher than those of PVP-HAN (64 m^2/g and 0.13 mL/g) (Figure 2b,c).

Before demonstrating Dox/FDz loading/releasing profiling and Dox/FDz/NIR chemo-thermo-gene multitherapy, we investigated photothermal effect of PVP-SPAN in comparison with PVP-HAN. In a cell-free cuvette, PVP-HAN and PVP-SPAN showed significant temperature elevation (ΔT = 34.4 and 57.6 °C, respectively) in comparison with controls of distilled water and template PVP-AgNP (ΔT = 5.8 and 9.8 °C,

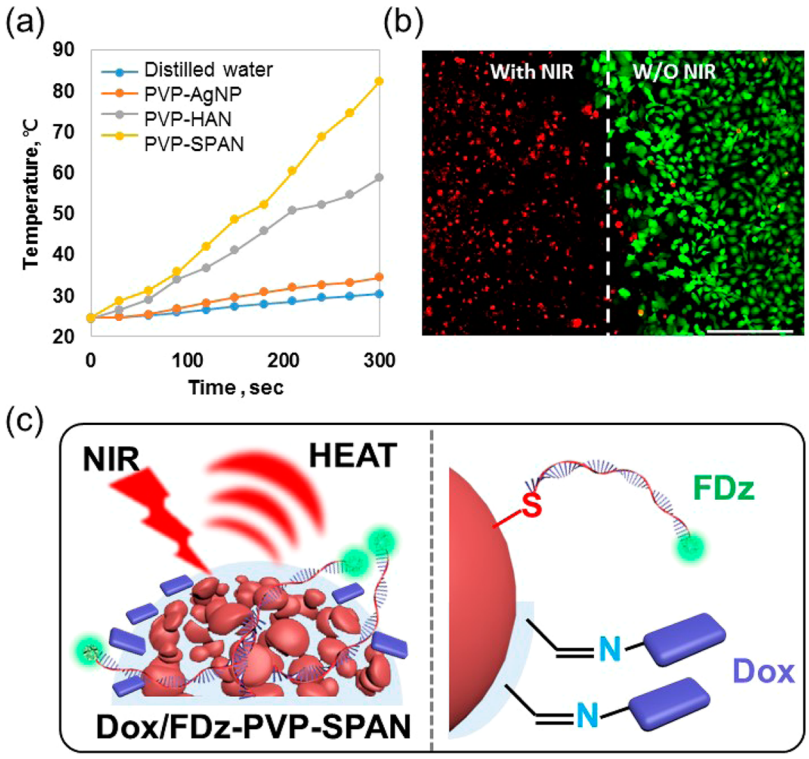

Figure 3. NIR irradiation mediated photothermal conversion effect and schematic illustration of dual drug-PVP-SPAN complex formation with loading strategy for therapeutic applications. (a) In cuvette assay, both PVP-SPAN and PVP-HAN exhibited highly efficient photothermal conversion mediated temperature elevation compared to controls. In specific, the temperature increment of PVP-SPAN was 2-fold higher than PVP-HAN. (b) The hyperthermia efficiency of PVP-SPAN in the Luc-Neo NS3 replicon RNA containing Huh7 cell lines. Region selective hyperthermia was induced in the designated area. The scale bar is 100 μm. (c) Schematic illustration of Dox/FDz loading strategy. Dox and FDz were loaded by two different strategies: Schiff base imine linkage between amine (Dox) and aldehyde (chemically introduced PVP coating layer) and affinity mediated adsorption between Au surface (spherically clustered nanoparticles) and thiol (thiolated FDz).

respectively) under the irradiation of 808 nm NIR laser (8 W/cm^2, 5 min). Higher photothermal conversion of PVP-SPAN relative to PVP-HAN could be originated from stronger absorption in the NIR region. In the human liver cells carrying HCV replicon (Luc-Neo NS3 replicon Huh7)[23] treated with PVP-SPAN, area selective hyperthermia was observed in the irradiated region with 808 nm laser (Figure 3a,b).

To load therapeutic cargos to the prepare nanoparticles, we introduced aldehyde groups onto surface PVP of PVP-SPAN, and PVP-HAN by previously reported method using glutaraldehyde.[24,25] After purification, loading of Dox and the thiolated FDz was performed by Schiff base linkage and thiol-Au formation, respectively (Figure 3c). The loading capacity of Dox and FDz to PVP-HAN and PVP-SPAN was then estimated by measuring UV−vis absorption of supernatant containing unloaded remaining Dox and FDz. Loading capacity of Dox to PVP-HAN and PVP-SPAN was 57,300 and 61,300 per nanoparticle, respectively, showing similar capacity. However, in case of FDz, PVP-SPAN exhibited 10 times higher loading capacity (253,900 FDz/PVP-SPAN) than that of PVP-HAN (27,500 FDz/PVP-HAN) (Figure 4a,b). The significant difference in loading capacity of FDz could be due to the differences in exposed gold surface area and structure. Co-loading of Dox and FDz was successfully performed, showing less than 20% of payload decrease compared to single drug loading (52,200 Dox and 22,300 FDz per PVP-HAN, 51,100 Dox and 209,700 FDz per PVP-SPAN) (Figures 4c and S3). Preferential release of the loaded Dox and FDz was observed depending on environment in which pH decreases from 7.4 to 5 induced the release of mainly Dox by cleavage of imine linkage and addition of glutathione as a reducing agent promoted release of FDz from gold surface (Figure 4d).

The cytotoxicity of PVP-HAN, PVP-AEN, and PVP-SPAN toward Luc-Neo NS3 replicon Huh7 cells was next assessed by the MTT cell viability assay and live/dead staining. In both assays, PVP-SPAN showed much lower cytotoxicity than PVP-AEN in all concentrations, suggesting that etching process removed cytotoxic silver and AgCl from PVP-AEN. We carried out all cell-based studies for the evaluation of therapeutic efficacy at concentrations of nanoaparticles which ensure more than 90% of cell viability throughout the present study (<25 pM of PVP-HAN and PVP-SPAN) (Figure S4).

We next evaluated efficacy of multimodal therapy using 25 pM of PVP-HAN (1.31 μM Dox and 0.56 μM FDz) and 25 pM of PVP-SPAN (1.28 μM Dox and 5.24 μM FDz) in the Luc-Neo NS3 replicon Huh7 cells, which were prepared under the same conditions for drug

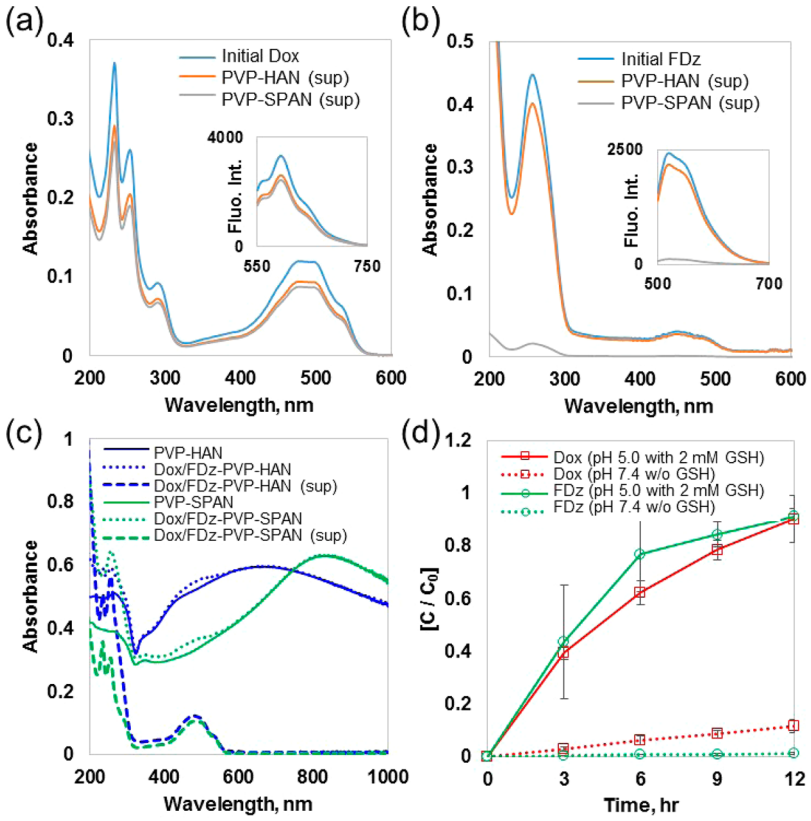

Figure 4. Loading and release profile of Dox and FDz in PVP-HAN and PVP-SPAN. Absorption spectra of (a) Dox and (b) FDz in the supernatant after incubation for loading. Inset shows fluorescence spectra of each supernatant. (c) UV−vis spectra of Dox/FDz loaded PVP-HAN and PVP-SPAN compared with the spectra of cargo-free PVP-HAN and PVP-SPAN clearly showed increase of distinctive absorbance around 260 and 480 nm. Amount of the loaded Dox and FDz was calculated by measuring absorbance of the remaining unloaded cargo in supernatant (Figure 3S). (d) Loaded Dox and FDz were gradually released under acidic (pH 5) and reducing (2 mM glutathione, GSH) environment.

loading. As expected, Dox-loaded nanoparticles showed a similar decrease in cell viability (53.3 and 51.1% for PVP-HAN and PVP-SPAN, respectively). However, PVP-SPAN mediated delivery of FDz and Dox/FDz reduced cell viabilities (FDz: 25.5% and Dox/FDz codelivery: 6.4%) more effectively than PVP-HAN mediated delivery (FDz: 66.5% and Dox/FDz: 35.2%) (Figure 5a). In case of FDz, viability of Luc-Neo NS3 replicon Huh7 cells was expected to decrease by FDz-mediated NS3 gene knockdown. The fluorescence microscopy images of the Luc-Neo NS3 replicon Huh7 cells treated with Dox and/or FDz loaded PVP-HAN and PVP-SPAN suggested successful cellular uptake of corresponding cargos (Figure 5c). We next demonstrated chemo-thermo multitherapy by using 5 pM of PVP-SPAN loaded with Dox and/or FDz (0.25 μM Dox and 1.05 μM FDz) in which lower concentration of the PVP-SPAN was used to more clearly observe the synergistic effect of the NIR irradiation for photothermal conversion. PVP-SPAN mediated delivery of Dox, FDz and Dox/FDz reduced cell viabilities down to 73.9, 58.3, and 24.2%, respectively. Controls with the cells treated with free Dox and/or FDz without nanoparticles presented little decrease in viability (88.1, 93.4, and 86.6% for Dox, FDz, and Dox/FDz, respectively). Finally, 808 nm NIR irradiation (1 W/cm^2, 5 min) to the cells treated with Dox/FDz-PVP-SPAN dramatically reduced cell viability down to 9.5% (Figure 5b).

CONCLUSION

In conclusion, PVP-SPAN was synthesized by temperature-dependent partial inhibition of galvanic replacement reaction with sacrificial Ag nanoparticle precursors followed by an etching process for the first time. Low temperature environment lead to limited replacement by inducing AgCl deposition on the Ag surface, resulting in the embedded spherical small Au nanoparticles. Subsequent addition of hydrogen peroxide induced etching of remaining Ag element and temperature elevation mediated dissolving of AgCl. The prepared PVP-SPAN exhibited porous structure with high surface-to-volume ratio and intense absorption in NIR region. We employed the PVP-SPAN for chemo-thermo-gene multitherapy after loading small molecule drug (Dox) and oligonucleotide drug (FDz) *via* independent surface chemistry. We successfully demonstrated the highly effective multimodal therapy in human liver cells carrying hepatitis C virus NS3 replicon as a model system of hepatitis C with Dox-FDz-loaded PVP-SPANs in combination with NIR

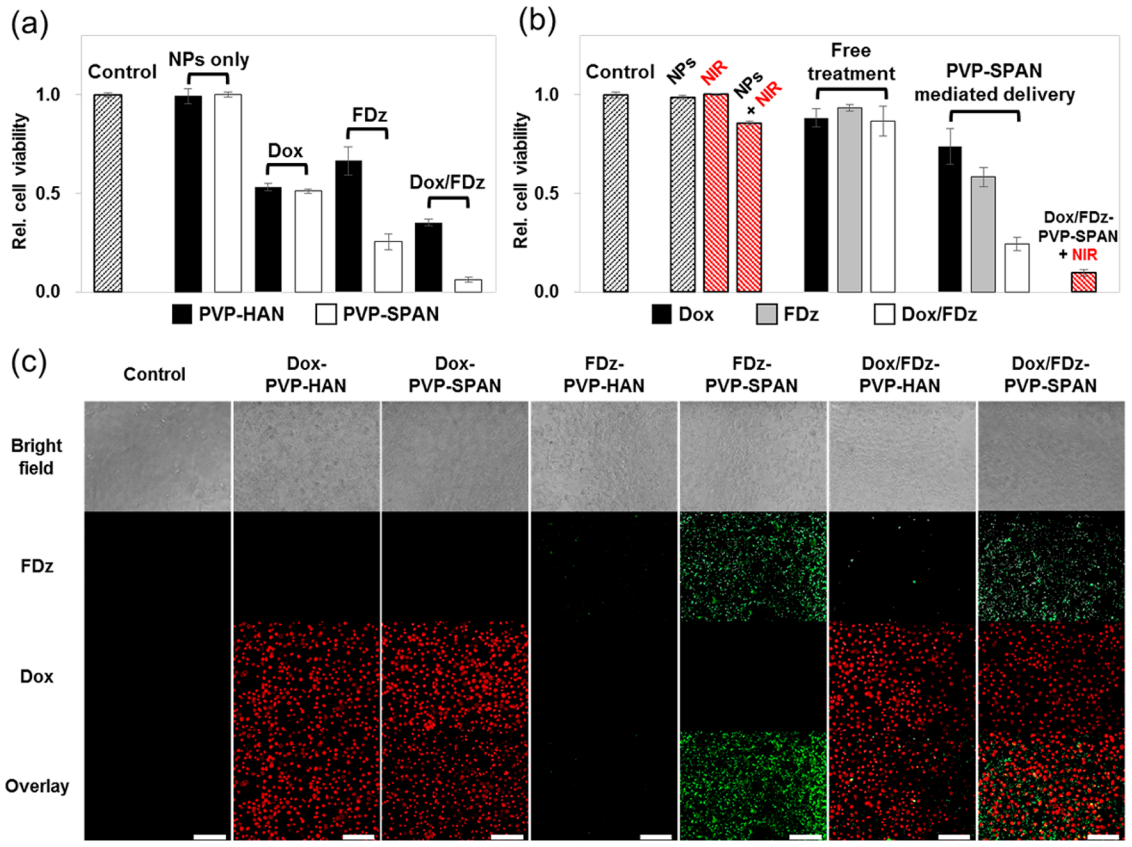

Figure 5. Quantitative evaluation of therapeutic efficacy of Dox and/or FDz loaded PVP-HAN and PVP-SPAN in NS3 replicon Huh7 cells. (a) Comparison of cell viability of NS3 replicon Huh7 cells treated with PVP-HAN, PVP-SPAN, Dox-loaded PVP-HAN, Dox-loaded PVP-SPAN, FDz-loaded PVP-HAN, FDz-loaded PVP-SPAN, Dox/FDz-loaded PVP-HAN, and Dox/FDz-loaded PVP-SPAN. (b) Synergistic chemo-thermo therapeutic efficacy was observed by using Dox and FDz loaded PVP-SPAN. PVP-SPAN mediated FDz/Dox delivery in combination with NIR irradiation showed significantly enhanced therapeutic efficacy. However, in control experiments, cells treated with only PVP-SPAN, NIR irradiation, and free Dox and/or FDz showed no notable decrease in viability. (c) Fluorescence microscopy images of the cells treated with the nanoparticles showed the successful delivery of the loaded Dox and/or FDz. Scale bars are 50 μm.

irradiation. We expect that the present porous Au−Ag nanoparticle will be widely applicable to biomedical research area due to its straightforward preparation, large surface area for high drug loading capacity, and NIR responsive photothermal property in the future.

METHODS

Materials. Hydrogen tetrachloroaurate (III) hydrate was purchased from Kojima Chemicals Co. (Japan). 3-(4,5-dimethylthiazol-2-yl)-2,5-diphenyl tetrazolium bromide (MTT), doxorubicin hydrochloride, silver nitrate, glutaraldehyde, and polyvinylpyrrolidone (MW 40 kDa) were purchased from Sigma (U.S.A.). Sodium bicarbonate, sodium hydroxide, and hydrogen peroxide (30%) were purchased from Junsei (Japan). 10× phosphate-buffered saline (PBS), Dulbecco's modified eagle's medium (DMEM), and fetal bovine serum (FBS) were purchased from WelGENE (Korea). LIVE/DEAD Viability/Cytotoxicity Assay Kit was purchased from Molecular Probes Invitrogen (U.S.A.). G418 was purchased from A. G. Scientific, Inc. (U.S.A.). All chemicals were used as received.

FAM-labeled thioloated DNAzyme (FAM-Dz-SH, FDz) which was designed to silence HCV NS3 gene was prepared as 5′-FAM-AAT GGG GAG GCT AGC TAC AAC GAG GCT TTG C-3′-SH and purchased from Genotech (Seoul, Korea). The underlined letters indicate catalytic motif of DNAzyme.

Synthesis of PVP-AgNP, PVP-HAN, PVP-AEN, and PVP-SPAN. *Synthesis of 100 nm Sized PVP-AgNP.* First, PVP (500 mg) was dissolved in ethylene glycol (30 mL) by sonication and vortex. The prepared PVP solution was heated to 170 °C followed by addition of 480 mg of silver nitrate dissolved in 30 mL of ethylene glycol solution. The reaction mixture was boiled for 2 h with vigorous stirring. The reaction mixture was then cooled to room temperature. The product was rinsed with distilled water 4 times using centrifugation at 8000 rpm for 20 min by Centrifuge 5810R (Eppendort, Germany). Finally, PVP-AgNP was redispersed in 200 mL of distilled water and stored in the dark.

Preparation of PVP-HAN by Galvanic Replacement Reaction. To 1 mL of the prepared 100 pM PVP-AgNP, 50 μL of 1 mM hydrogen tetrachloroaurate (III) hydrate stock was added at 80 °C. After addition of Au (III) solution, the mixed solution was incubated for 30 min with stirring. When the color of the reaction mixture did not show any further change, the mixture was rinsed with distilled water 4 times using centrifugation at 8000 rpm for 20 min each. The final product was characterized by UV−vis spectrophotometry and stored at room temperature.

Preparation of PVP-AEN by Inhibitory Galvanic Replacement Reaction. To 1 mL of the prepared 100 pM PVP-AgNP, 50 μL of 1 mM hydrogen tetrachloroaurate (III) hydrate stock was added at 4 °C. After addition of Au (III) solution, the mixed solution was incubated for 30 min with stirring. When the color change finished, the mixture was rinsed with distilled water 4 times

using centrifugation at 8000 rpm for 20 min each. The final product was characterized by UV−vis spectrophotometry and stored at room temperature.

Preparation of PVP-SPAN by Hydrogen Peroxide Etching. To 1 mL of the as-synthesized 100 pM PVP-AENs, 2 mL of 30% hydrogen peroxide was added in ambient conditions. The mixed solution started to form bubbles with intense heat generation, and the color changed rapidly. After 10 min, the mixture was rinsed with distilled water 4 times using centrifugation at 8000 rpm for 20 min each. The final product was characterized by UV−vis spectrophotometry and stored at room temperature.

Characterization of the Prepared PVP-AgNPs, PVP-HANs, PVP-AENs, and PVP-SPANs. Energy-filtering transmission electron microscope LIBRA 120 (Carl Zeiss, Germany), high-resolution TEM, and HAADF-STEM Tecnai F20 (FEI, Netherlands) were used to obtain images of nanoparticles. UV−vis spectrophotometer S-3100 (Scinco, Korea) and SynergyMx (Biotek, UK) were used to obtain UV−vis absorption spectra. Fluorescence was measured by spectrofluorometer FP-8300 (Jasco Inc., U.S.A.). Energy dispersive spectroscopy was carried out by using EDAX (U.S.A.). Nitrogen adsorption isotherms were measured in a NOVA sorption apparatus. Surface area calculations were carried out using the BET method, and the pore size distribution was calculated according to the BJH method. 808 nm NIR irradiation was performed by surgical laser accessories OCLA (Soodogroup Co., Korea). Cell images were taken using an In cell analyzer 2000 (GE healthcare, U.S.A.) and Ti inverted fluorescence microscope equipped with a 60× (1.4 numerical aperture) objective (Nikon Co., Japan) and a CoolSNAP cf charge-coupled device (CCD) camera (Photometrics, U.S.A.) and BX51 M optical microscope (Olympus Co., Japan) equipped with fluorescence light source and filters.

Characterization of Photothermal Effect. *Temperature Elevation Measurement.* To assess the temperature elevation by photothermal conversion, 1 mL of 200 pM of PVP-AgNP, PVP-HAN, PVP-SPAN, and control distilled water were placed in 2 mL tubes. The 808 nm NIR laser was irradiated to each solution with intensity of 0.4 W/cm^2 for 5 min, and the temperature change was measured by a digital thermometer in every 30 s.

Cell-Based Hyperthermia Measurement. To examine hyperthermia by photothermal conversion, PVP-SPAN in 1× PBS was treated to NS3 replicon Huh7 cells in a 6-well plate that were seeded with confluency of 50,000 cells/well. After 3 h of incubation in a humidified 5% CO_2 incubator at 37 °C, residual PVP-SPAN was removed and washed with 1× PBS two times, followed by replacing with serum-containing media. Next, the cells were irradiated with 808 nm NIR laser with intensity of 8 W/cm^2 for 5 min at ambient condition and incubated for additional 2 h. Following incubation, 200 μL of the combined live−dead cell staining solution (2 μM calcein AM and 4 μM EthiD-1 in D-PBS) was added to each well and incubated for 15 min for staining. Fluorescent images of the cells were obtained using an In cell analyzer.

Introduction of Aldehyde Functional Group onto PVP Coating of PVP-HAN and PVP-SPAN. *Introduction by Claisen−Schmidt Reaction.* To 1 mL of the prepared 100 pM PVP-HAN and PVP-SPAN, 100 μL of 1 mM glutaraldehyde stock solution in distilled water was added. Sodium bicarbonate was added to final concentration of 1 mM and set pH to 9. The mixed solution was incubated for 1 h with shaking at room temperature. After the reaction, the mixture was rinsed with distilled water 4 times using centrifugation at 8000 rpm for 20 min each. The final product was characterized by UV−vis spectrophotometry and stored at room temperature.

Quantitative Measurement of Loading and Release of Dox and FDz. *Dox Loading on PVP-HAN and PVP-SPAN by Schiff Base Imine Linkage formation.* Briefly, 10 μL of 1 mM Dox in distilled water stock solution was added to 1 mL of 100 pM PVP-HAN and PVP-SPAN and inverted for 20 s. To form the Schiff base imine bond, pH of mixture was set to 10 by addition of sodium hydroxide solution. The reaction mixture was incubated for 12 h with on a shaking plate at room temperature with a cover to block light. The unbound substrate was removed by centrifugation at 8000 rpm for 20 min each and washed with distilled water four times. Finally, Dox-loaded PVP-HAN and PVP-SPAN were redispersed in distilled water and stored in the dark. Calculation of loaded Dox was performed by UV−vis spectrophotometer with reported extinction coefficient ($\varepsilon_{Dox,\ 480\ nm}$ = 11,500 L mol^{-1} cm^{-1}) based on Lambert−Beer's law.

FAM-Dz-SH Loading on PVP-HAN and PVP-SPAN by Self-Assembled Monolayer Formation. Ten μL of 1 mM FAM-Dz-SH (FDz) in distilled water stock solution was added to the 1 mL of 100 pM PVP-HANs and PVP-SPANs. To achieve the loading of FDz to PVP-HAN and PVP-SPAN, the reaction mixture was incubated for 12 h on a horizontal shaker at room temperature in dark. The unbound substrate was removed by centrifugation at 8000 rpm for 20 min each and washed with distilled water four times. Finally, FDz loaded PVP-HAN and PVP-SPAN were redispersed in 1 mL of 1× PBS. Calculation of loaded FDz was based on absorption measured by using UV−vis spectrophotometer and extinction coefficient of FDz ($\varepsilon_{FDz,\ 260\ nm}$ = 8.86 × 10^5 L mol^{-1} cm^{-1}). Because of the very low absorption of FAM, we calculated loading capacity based on absorption of nucleobases of FDz.

Simultaneous Loading of Dox/FDz on PVP-HAN and PVP-SPAN. The mixture of 10 μL of 1 mM FDz and 10 μL of 1 mM Dox in distilled water stock solution was sequentially added to the 1 mL of 100 pM PVP-HAN and PVP-SPAN. The reaction mixture was then incubated for 12 h on a horizontal shaker at room temperature in dark. The unbound substrate was removed by centrifugation at 8000 rpm for 20 min and washed with distilled water four times. Finally, Dox/FDz coloaded PVP-HAN and PVP-SPAN were redispersed in 1 mL of 1× PBS.

Dox and FDz Release Profile at Different pHs (pH 5.0 and 7.4) and Reductive Environment (with and without 2 mM glutathinone) Condition. To monitor the selective release of the loaded Dox and FDz under cancer cell imitated conditions, the Dox/FDz-PVP-SPAN were dispersed in citrate buffer (pH 5.0) and phosphate buffered saline (pH 7.4) solution with/without 2 mM glutathione at room temperature. At every 3 h during 12 h of observation, the solution of Dox/FDz-PVP-SPAN was centrifuged at 14,000 rpm for 5 min by Centrifuge 5418 (Eppendorff, Germany) to pull down the nanocomplex, and the amount of the released Dox and FDz were determined by measuring absorbance of supernatant at 260 and 480 nm, respectively. The Dox and FDz concentration of supernatant was calculated by equations from the premeasurement of free Dox and FDz to avoid absorbance overlapping mediated error.

Cellular Uptake. *Fluorescence Image of Cells Treated with Dox and/or FDz Loaded PVP-HANs and PVP-SPANs.* The Dox and/or FDz loaded PVP-HANs and PVP-SPANs in 1× PBS were treated to the cultured Luc-Neo NS3 replicon Huh7 cells with a density of 10,000 cells per well in a 96-well culture plate. After the treatment, the cells were incubated for 3 h in a humidified incubator with 5% CO_2 at 37 °C. Residual nanomaterials were removed and washed with 1× PBS followed by replacing with fresh serum-containing media. [To observe NIR irradiation mediated therapeutic efficacy, the cells were incubated for additional 1 h after irradiation with a 808 nm NIR laser.] Finally, the cells were observed by an In cell analyzer.

Cell Viability Assay. *Cell Culture.* The human hepatoma cell line Huh7 containing NS3 hepatitis C virus RNA was grown in DMEM containing 4.5 g/L D-glucose, supplemented with 10% FBS, 100 units/mL penicillin, 100 mg/mL streptomycin, and 500 μg/mL of G418. The cells were grown in a humidified 5% CO_2 incubator at 37 °C.

MTT Assay for Cell Viability Measurement. MTT powder was dissolved in 1× PBS at 5 mg/mL concentrations and filtered through a 0.2 μm pore sized sterilized syringe filter. The stock solution was stored at 4 °C. The NS3 replicon Huh7 cells were seeded with a density of 10,000 cells per well of a 96-well culture plate with 100 μL of growth media (about 50−70% confluency).

(i) To compare the PVP-HANs and PVP-SPANs mediated drug delivery efficiency, the cells were treated with free Dox, free FDz, Dox and/or FDz loaded PVP-HAN, and Dox and/or FDz loaded PVP-SPAN and incubated for 24 h at 37 °C. Then, the cells were rinsed with 1× PBS. Twenty μL MTT stock solution was added to the cells and incubated for 2−4 h until a purple color developed to detect the metabolically active cells. The media was discarded, and

200 μL DMSO was added to each well to make water-insoluble formazan salt solubilized. Then, the optical densities of each well in the plates were measured at 560 nm. Mean and standard deviation of triplicates were calculated and plotted.

(ii) To investigate the synergistic effect of NIR irradiation with PVP-SPAN-based chemotherapy, after cells were treated with free Dox, free FDz, free PVP-SPANs, Dox and/or FDz loaded PVP-SPAN with or without NIR irradiation, the cells were incubated for 24 h at 37 °C. Then, the cells were rinsed with 1× PBS. Twenty μL MTT stock solution was added to detect the metabolically active cells, and the cells were incubated for 2−4 h until a purple color developed. The media was discarded, and 200 μL DMSO was added to each well to make water-insoluble formazan salt solubilized. Then, the optical densities of each well in the plates were measured at 560 nm. Mean and standard deviation of triplicates were calculated and plotted.

LIVE/DEAD Cell Staining. The cytotoxicity of PVP-HAN, PVP-AEN, and PVP-SPAN and hyperthermia effect of PVP-SPANs were estimated by using the LIVE/DEAD Viability/Cytotoxicity Assay Kit. The Luc-Neo NS3 replicon Huh7 cells were seeded at 10,000 cells per well of a 96-well cell culture plate and 50,000 cells per well of a 6-well cell culture plate. The cells were incubated with the nanoparticles at designated concentrations in 1× PBS for 4 h and then replaced with fresh media and incubated for 20 h. Following incubation, 50 μL (96 well) or 200 μL (6 well) of the live−dead cell staining solution (2 μM calcein AM and 4 μM EthiD-1 in D-PBS) was added to each well and incubated for 30 min. Images were obtained using a microscope equipped with fluorescence light source and filters.

Conflict of Interest: The authors declare no competing financial interest.

Acknowledgment. This work was supported by the Basic Science Research Program (2011-0017356), International S&T Cooperation Program (2014K1B1A1073716) and the Research Center Program (IBS-R008-D1) of IBS (Institute for Basic Science) through the National Research Foundation of Korea (NRF) and Research Program (C0193918) through the SMBA funded by the Korean government (MEST).

Supporting Information Available: Additional analytical data. This material is available free of charge *via* the Internet at http://pubs.acs.org.

REFERENCES AND NOTES

1. Sun, Y.; Mayer, B. T.; Xia, Y. Template-Engaged Replacement Reaction: a One-Step Approach to the Large-Scale Synthesis of Metal Nanostructures with Hollow Interiors. *Nano Lett.* **2002**, *2*, 481–485.
2. Sun, Y.; Wiley, B.; Li, Z.-Y.; Xia, Y. Synthesis and Optical Properties of Nanorattles and Multiple-Walled Nanoshells/Nanotubes Made of Metal Alloys. *J. Am. Chem. Soc.* **2004**, *126*, 9399–9406.
3. Sun, Y.; Xia, Y. Multiple-Walled Nanotubes Made of Metals. *Adv. Mater.* **2004**, *16*, 264–268.
4. Jang, H.; Kim, Y.-K.; Huh, H.; Min, D.-H. Facile Synthesis and Intraparticle Self-Catalytic Oxidation of Dextran-Coated Hollow Au-Ag Nanoshell and Its Application for Chemo-Thermotherapy. *ACS Nano* **2014**, *8*, 467–475.
5. Hirsch, L. R.; Jackson, J. B.; Lee, A.; Halas, N. J.; West, J. L. A Whole Blood Immunoassay using Gold Nanoshells. *Anal. Chem.* **2003**, *75*, 2377–2381.
6. Jackson, J. B.; Westcott, S. L.; Hirsch, L. R.; West, J. L.; Halas, N. J. Controlling the Surface Enhanced Raman Effect *via* the Nanoshell Geometry. *Appl. Phys. Lett.* **2003**, *82*, 257–279.
7. You, J.; Zhang, G.; Li, C. Exceptionally High Payload of Doxorubicin in Hollow Gold Nanospheres for Near-Infrared Light-Triggered Drug Release. *ACS Nano* **2010**, *4*, 1033–1041.
8. Melancon, M. R.; Lu, W.; Yang, Z.; Zhang, R.; Cheng, Z.; Elliot, A. M.; Stafford, J.; Olson, T.; Zhang, J. Z.; Li, C. *In Vitro* and *In Vivo* Targeting of Hollow Gold Nanoshells Directed at Epidermal Growth Factor Receptors for Photothermal Ablation Therapy. *Mol. Cancer Ther.* **2008**, *6*, 1730–1739.
9. Skrabalak, S. E.; Au, L.; Li, X. D.; Xia, Y. Facile Synthesis of Ag Nanocubes and Au Nanocages. *Nat. Protoc.* **2007**, *2*, 2182–2190.
10. Smigelskas, A. D.; Kirkendall, E. O. Zinc Diffusion in Alpha Brass. *Trans. Am. Inst. Min. Metall. Eng.* **1947**, *171*, 130–142.
11. Mahmoud, M. A.; Saira, F.; El-Sayed, M. A. Experimental Evidence for the Nanocages Effect in Catalysis with Hollow Nanoparticles. *Nano Lett.* **2010**, *10*, 3764–3769.
12. Mahmoud, M. A.; Narayanan, R.; El-Sayed, M. A. Enhancing Colloidal Metallic Nanocatalysis: Sharp Edges and Corners for Solid Nanoparticles and Cage Effect for Hollow Ones. *Acc. Chem. Res.* **2013**, *46*, 1795–1805.
13. Cobley, C. M.; Au, L.; Chen, J.; Xia, Y. Targeting Gold Nanocages to Cancer Cells for Photothermal Destruction and Drug Delivery. *Expert Opin. Drug Delivery* **2010**, *7*, 577–587.
14. Yavuz, M. S.; Cheng, Y.; Chen, J.; Cobley, C. M.; Zhang, Q.; Rycenga, M.; Xie, J.; Kim, C.; Song, K. H.; Schwartz, A. G.; Wang, L. V.; Xia, Y. Gold Nanocages Covered by Smart Polymers for Controlled Release with Near-Infrared Light. *Nat. Mater.* **2009**, *8*, 935–939.
15. Hu, M.; Chen, J.; Li, Z.-Y.; Au, L.; Hartland, G. V.; Li, X.; Marquez, M.; Xia, Y. Gold Nanostructures: Engineering Their Plasmonic Properties for Biomedical Applications. *Chem. Soc. Rev.* **2006**, *35*, 1084–1094.
16. Liu, G.; Feng, D.-Q.; Zheng, W.; Chen, T.; Li, D. An Anti-Galvanic Replacement Reaction of DNA Template Silver Nanoclusters Monitored by the Light-Scattering Technique. *Chem. Commun.* **2013**, *49*, 7941–7943.
17. Wu, Z. Anti-Galvanic Reduction of Thiolated-Protected Gold and Silver Nanoparticles. *Angew. Chem., Int. Ed.* **2012**, *51*, 2934–2938.
18. Liu, Y.; Hight Walker, A. R. Preferential Outward Diffusion of Cu during Unconventional Galvanic Replacement Reaction between $HAuCl_4$ and Surface-Limited Cu Nanocrystals. *ACS Nano* **2011**, *5*, 6843–6854.
19. Zhang, W.; Yang, J.; Lu, X. Tailoring Galvanic Replacement Reaction for the Preparation of Pt/Ag Bimetallic Hollow Nanostructures with Controlled Number of Voids. *ACS Nano* **2012**, *6*, 7397–7405.
20. Santoro, S. W.; Joyce, G. F. A General Purpose RNA-Cleaving DNA Enzyme. *Proc. Natl. Acad. Sci. U.S.A.* **1997**, *94*, 4262–4266.
21. Santoro, S. W.; Joyce, G. F. Mechanism and Utility of an RNA-Cleaving DNA Enzyme. *Biochemistry* **1998**, *37*, 13330–13342.
22. Im, S. H.; Lee, Y. T.; Wiley, B.; Xia, Y. Large-Scale Synthesis of Silver Nanocubes: the Role of HCl in Promoting Cube Perfection and Monodispersity. *Angew. Chem., Int. Ed.* **2005**, *44*, 2154–2157.
23. Lohmann, V.; Korner, F.; Koch, J.; Herian, U.; Theilmann, L.; Bartenschlager, R. Replication of Subgenomic Hepatitis C Virus RNAs in a Hepatoma Cell Line. *Science* **1999**, *285*, 110–113.
24. Rodriguez-Lorenzo, L.; de la Rica, R.; Alvarez-Puebla, A.; Liz-Marzan, L. M.; Stevens, M. M. Plasmonic Nanosensors with Inverse Sensitivity by Means of Enzyme-Guided Crystal Growth. *Nat. Mater.* **2012**, *11*, 604–607.
25. Kobayashi, K.; Okamoto, I.; Morita, N.; Kiyotani, T.; Tamura, O. Synthesis of the Proposed Structure of Phaeosphaeride A. *Org. Biomol. Chem.* **2011**, *9*, 5825–5832.